IEEE Access
Multidisciplinary | Rapid Review | Open Access Journal

Received April 19, 2021, accepted May 10, 2021, date of publication May 19, 2021, date of current version June 24, 2021.

Digital Object Identifier 10.1109/ACCESS.2021.3081822

Millimeter-Wave Propagation Measurement and Modeling in Indoor Corridor and Stairwell at 26 and 38 GHz

YUYAN SHEN[1], YU SHAO[1,2], (Member, IEEE), XI LIAO[1], (Member, IEEE), HENG ZHANG[1], AND JIE ZHANG[1,2], (Senior Member, IEEE)

[1]School of Communication and Information Engineering, Chongqing University of Posts and Telecommunications, Chongqing 400065, China
[2]Department of Electronic and Electrical Engineering, The University of Sheffield, Sheffield S10 2TN, U.K.

Corresponding author: Yu Shao (shaoyu@cqupt.edu.cn)

This work was supported in part by the National Natural Science Foundation of China under Grant 61701061 and Grant 61801062, in part by the National Key Research and Development Program of China under Grant 2017YFE0118900, in part by the Natural Science Foundation of Chongqing under Grant cstc2019jcyjmsxmX0606, and in part by the European Union's H2020-MSCA-IF-GATE under Grant 843133.

ABSTRACT Accurate propagation characteristics are essential for future indoor millimeter-wave (mmWave) small cell network planning. This paper presents propagation measurements at 26 GHz and 38 GHz which are important candidate bands for fifth generation mmWave communication. Measurements are conducted in an indoor corridor, as well as a stairwell whose mmWave channel is seldom investigated before. In these measurements, an omnidirectional biconical antenna is used as transmitter and a steerable directional horn antenna is used as receiver. The directional and omnidirectional path loss exponents, shadow factors, cross-polarization discrimination ratios and root-mean-square delay spreads are analyzed for both line-of-sight and non-line-of-sight scenarios in both co-polarization and cross-polarization, and these characteristics are compared for different frequencies and environments. It is found obvious depolarization phenomenon in non-line-of-sight scenario for higher frequency. Compared to the corridor, the stairwell has larger path loss exponents and root-mean-square delay spreads, and the depolarization is also more evident in stairwell. The results in this paper are beneficial to building efficient and robust indoor mmWave communication systems.

INDEX TERMS Millimeter-wave, indoor propagation, path loss, cross-polarization discrimination ratio, delay spread.

I. INTRODUCTION

With the advent of fifth generation (5G) mobile communication era and the popularity of internet of things (IoT) technology, the wireless data traffic grows exponentially [1]. Particularly, the demand of data rate in indoor environment is urgent since plenty of wireless communications services take place indoors. As the spectrum resources below 6 GHz are almost exhausted, millimeter-wave (mmWave) spectrum where a large amount of raw bandwidth is available will be exploited and utilized to alleviate the traffic crunch [2]. According to the regulations of 3GPP and ITU WRC-15, 26 GHz, 28 GHz, 38 GHz, and 60 GHz are some of the most important bands in mmWave communication [3]. So far, several trials have been executed in some countries to demonstrate the mmWave network in real field [4]. However, mmWave suffers from larger propagation loss than lower frequency, which confines the coverage area of mmWave network. Thus, dense small-cell or hotspot deployment for mmWave network, which is expected in future indoor communication systems, is a promising way to alleviate path loss and satisfy the huge capacity demand in indoor environment. Due to the complex building structure and small wavelength, phenomena such as shadowing, multipath and depolarization will occur in mmWave indoor propagation, which have a great impact on system performance [5]. To design a capable and robust mmWave communication system, propagation characteristics and models should be studied deeply in various indoor environments.

Since 1990's, especially in the last decades, many researches on mmWave channel measurement and modeling have been conducted in Ka band, V band, and E band.

The associate editor coordinating the review of this manuscript and approving it for publication was Matti Hämäläinen.

Two path loss models at 83.5 GHz were presented and compared in four indoor environments in [6], while indoor wideband channel characteristics were measured in the 59-65 GHz and 80.5-86.5 GHz band in [7]. In [8], cross-polarization ratios were measured in indoor 70 GHz channels. 60 GHz is one of the most promising band which has attracted attentions for a long time. The delay spread and polarization dependence of indoor propagation at around 60 GHz were studied in [9] and [10], respectively. In [11] and [12], indoor mmWave channel at 60 GHz were measured and analyzed by ray tracing method, and it was found that the dominant propagating path are line-of-sight (LOS) path, first-order and second-order reflection paths, however the roles of diffraction were controversial in these two works. Clustering results for a double-directional 60 GHz MIMO channel were presented in [13], and a measurement-based statistical spatiotemporal radio channel model was proposed in [14]. Recently extensive channel measurements in 3-D space in office at 60 GHz were conducted, and an extended Saleh–Valenzuela model with both delay and angular cluster features was presented in [15]. Reference [16] investigated large scale fading characteristics such as path loss exponent (PLE), cross-polarization discrimination ratio (XPD), and shadowing factor at 45 GHz in three typical indoor environments. The non-line-of-sight (NLOS) channels in a confined in-building corridor in 41 GHz band were measured in [17]. In [18], the multipath dispersion characteristics of outdoor-to-indoor (O2I) propagation were presented in the angular and delay domains at 32 GHz. The most potential 5G mmWave candidates are 28 GHz and 38 GHz bands, and much pioneering researches on their propagation measurements and channel models have been done by researchers from New York University. Extensive indoor measurements at 28 GHz and 73 GHz have been conducted [19]-[22], both co-polarization and cross-polarization scenarios were measured, and both directional and omnidirectional path loss models were presented, furthermore seven path loss models were compared and analyzed. In [23], wideband mmWave outdoor propagation measurements and channel models at 28, 38, 60, and 73 GHz were first presented. Propagation characteristics of 28 GHz and 38 GHz were measured in various environments, including downtown area, railway station and airport [24], indoor dining room [25], office [26], and indoor corridor [27]–[29]. Small-scale spatiotemporal characteristics such as the delay spread, the azimuth/elevation angle spread of arrival and XPD were measured at 25.5, 28, 37.5, and 39.5 GHz for different polarimetric combinations in [30]. In [31], 28 GHz measurement campaigns were conducted in both indoor and outdoor environments in the United Arab Emirates. Massive path loss and direct gain measurements were carried out at 28 GHz in an indoor environment with corridor in [32]. The indoor propagation channel around 28 GHz were measured by massive uniform linear array (ULA) and uniform planar array (UPA) in [33], and by uniform cylindrical array (UCA) in [34]. O2I propagation channel at 28 GHz was measured and analyzed by phased array antennas in [35].

Although stairwells, which are vital for daily use especially for emergency applications, are essential parts in modern buildings, studies on the propagation in stair structure are relatively fewer than those in other indoor environments where extensive investigations have been conducted. In [36], propagation measurements in a multi-floor stairwell were carried out over the frequency range of 1.2 to 1.8 GHz, and a 3-D ray-polygon tracing propagation model was proposed. Radio propagation measurements in multifloor stairwell were conducted at 2.4 GHz and 5.8 GHz in [37]-[39], and an image-based ray tracing analysis revealed that in the studied case the impact of reflections from stairwell walls were limited but the transmissions through the stairs contributed the total received power most. Propagation in four typical stairwells was investigated and two path loss models were compared in [40], both vertical and horizontal polarizations were considered. It was found that the path loss model based on the so-called ''accumulative distance'' is more accurate than the model based on the conventional separation distance between transmitting and receiving antennas. In [41], path loss model for stairwell environment was presented based on the measurements at four different stairwells at 900 MHz and 1800 MHz. A deterministic ray-tracing model was presented for indoor stairwell channel at 10 GHz in [42], and the effects of diffraction and multiple diffractions from the edges of step were calculated using heuristic diffraction coefficients. Very recently, the propagation characteristics of stairwell in mmWave band at 26, 28, 32 and 38 GHz for various polarization combinations were measured and different path loss models were compared in [43], [44], and the channel parameters of stairwell were analyzed and compared at 3.5 GHz and 28 GHz in [45].

Despite the numerous existing studies mentioned above, more measurements on mmWave propagation taking polarization into account are still required in various indoor environments. Compared to outdoor propagation, multipath effects are more obvious in indoor environments such as corridor and stairwell, and the multiple reflection, diffraction, refraction and even diffuse scattering will lead to depolarization phenomenon. However, researches on polarization characteristics of mmWave are limited, particularly investigations on mmWave channel in stairwell are even rarer. To the best of our knowledge, the time dispersion characteristics of mmWave in stairwell have not been reported.

In this work, the channel of indoor corridor and stairwell at 26 GHz and 38 GHz are extensively measured, and the directional and omnidirectional PLEs, shadow factors, XPDs and root-mean-square (RMS) delay spreads are analyzed for both LOS and NLOS scenarios in both co-polarization and cross-polarization. The results in this paper are beneficial to building an efficient and reliable mmWave indoor small cell network. The corridor and stairwell environments, and the measurement setup and procedure are described in Section II. The path loss, cross-polarization discrimination ratio, and RMS delay spread results are presented in Section III, IV and V, respectively. Comparisons with

other related work are presented in Section VI. Finally, the conclusions are given in Section VII.

II. PROPAGATION MEASUREMENT CAMPAIGN

A. MEASUREMENT ENVIRONMENT DESCRIPTION

Measurements were carried out in an indoor corridor and indoor stairwell at 26 GHz and 38 GHz band, which are the most typical indoor environments and share similar structures among most modern buildings.

Fig. 1 shows the photos and layout of the indoor corridor. The corridor is in a "L" shape. Two transmitter (TX) locations (red dots in Fig. 1) and ten receiver (RX) locations (blue dots in Fig. 1) were selected and the propagating paths contained both LOS case and NLOS case. The RXs were lined up at the center of the corridor and the distance of the adjacent RXs was 0.6 m. There were LOS paths from TX1 to RXs, whereas all the paths from TX2 to RXs were NLOS since TX2 was obstructed by the corner. The corridor consists of concrete wall, tiled floor, plaster ceiling, glass window, and wooden door. All the doors and windows were closed during measurements.

(a)

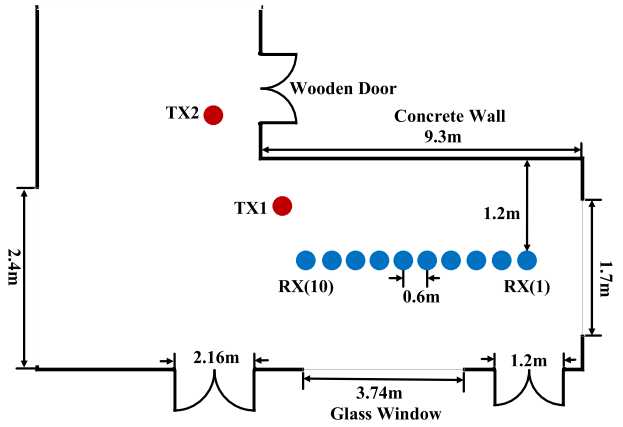

(b)

FIGURE 1. Corridor measurement layout with TX and RX locations. (a) Photos of the corridor environment; (b) Scaled layout of the corridor measurement.

Fig.2 shows the photos and geometries of the indoor stairwell. The measurements on stairwell were conducted on the second floor of a laboratory building. There are two sections of stair steps between the second and third floor, which are denoted as S1 and S2 in Fig. 2. The first section has 14 steps and the second section has 12 steps.

(a)

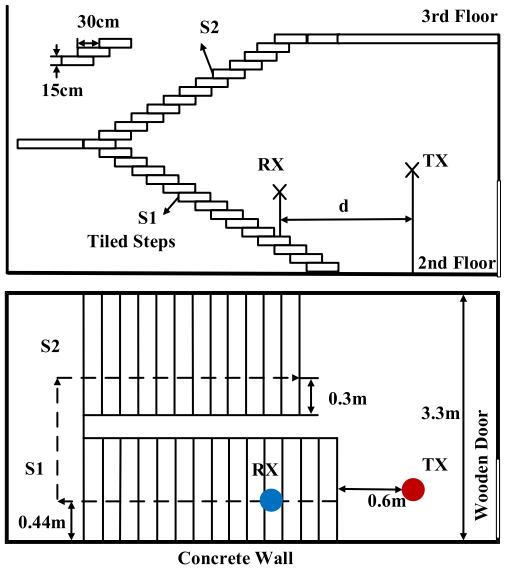

(b)

FIGURE 2. Stairwell measurement layout with TX and RX locations. (a) Photos of the stairwell environment; (b) Scaled layout of the stairwell measurement.

The depth (tread) and height (rise) of each step are 30 cm and 15 cm, respectively. During the measurements, the TX with a height of 1.8 m was fixed on the entrance platform of the second floor. RX with a height of 1.2 m was moved upward from the second floor to the third floor, and the adjacent RXs had two steps apart. There were LOS paths from TX to RX in S1 section, whereas all the paths from TX to RX in S2 section were NLOS. The stairwell is composed of tiled steps, concrete wall and ceiling, iron railings, and a wooden door which was kept closed during the measurements.

B. MEASUREMENT EQUIPMENT AND PROCEDURE

The channel sounder system used in the measurements is shown in Fig. 3. The system mainly consisted of a vector network analyzer (Keysight N5235B) which can measure the amplitude and phase of the channel transfer function. In addition, the vector network analyzer enables frequency sweep in a wide band which provides a high resolution in the delay domain. The sweeping frequency range was 24-28 GHz for 26 GHz band, and 36-40 GHz for 38 GHz band, which means the resolution in the delay domain was 0.25 ns. The TX antenna was an omnidirectional biconical antenna with

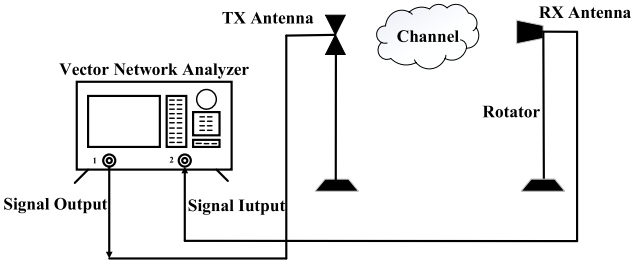

FIGURE 3. Channel sounder systems for indoor mmWave propagation measurement.

a gain of 4.8 dBi at 26 GHz and 6.0 dBi at 38 GHz, while the RX antenna was a directional horn antenna with a gain of 13.3 dBi at 26 GHz and 16.1 dBi at 38 GHz. The XPD of the antenna is 36 dB at 26 GHz, and 42 dB at 38 GHz, which is quite high so that its influence on polarization measurement is negligible. The antennas were fixed on rotatable tripods. The specifications of the channel sounding system are listed in Table 1.

TABLE 1. Specifications of the channel sounding system.

Center frequency	26 GHz	38 GHz
Environments	corridor, stairwell	
Frequency range	24-28 GHz	36-40 GHz
Transmitting power	0 dBm	
TX Antenna	omnidirectional biconical antenna	
TX Antenna Gain	4.8 dBi	6.0 dBi
TX Antenna HPBW (E)	40°	30°
TX Antenna HPBW (H)	360 °	
TX Antenna Height	1.4 m in corridor, 1.8 m in stariwell	
TX Polarization	vertical	
RX Antenna	directional horn antenna	
RX Antenna Gain	13.3 dBi	16.1 dBi
RX Antenna HPBW (E)	35°	30°
RX Antenna HPBW (H)	40°	30°
RX Antenna Height	1.4 m in corridor, 1.2 m in stariwell	
RX Polarization	vertical / horizontal	
RX azimuth sweeping step	36°	
Distance between adjacent RXs	0.6 m in corridor, 2 steps in stairwell	

In corridor, the heights of both TX and RX antennas were1.4 m. 10 RX positions were selected along a line with a spacing of 0.6 m between adjacent RXs. In stairwell, the heights of TX and RX antennas were 1.8 m and 1.2 m, respectively. RX antenna moved upward along the stair with a step of 2 stairs, and a total of 12 RX positions were measured. To obtain angular characteristics at each position, azimuth sweeping was performed on RX antenna with a sweeping step of 36° which is approximately equal to the half power beam width (HPBW) of RX antenna, and multiple local measurements with a separation of 1 cm were carried out at each azimuth angle to average the small-scale fading. To analyze the polarization characteristic of the channels, for each TX and RX combination two polarization configurations were measured: co-polarization (vertical-to-vertical, V-V) and cross-polarization (vertical-to-horizontal, V-H). The TX antenna was fixed to be vertical polarization, and the polarization state of RX antenna was switched between vertical and horizontal by rotating the horn antenna by 90°. For each TX-RX combination, the propagating path is classified into LOS and NLOS. For directional model, the path is regarded as LOS only if the TX and RX are aligned on boresight in azimuth and elevation planes, and meanwhile the path is not obstructed, otherwise the path is categorized to NLOS. For omnidirectional model, the path is LOS provided there is an unobstructed direct path between TX and RX, and NLOS means the path between TX and RX is blocked.

III. PATH LOSS RESULTS

Path loss is one of the most important parameters to characterize the large-scale fading of the channel. A widely used path loss model is the close-in free space reference distance (CI) path loss model which can be written as:

$$PL(d)[dB] = PL(d_0)[dB] + 10n log_{10}(\frac{d}{d_0}) + \chi_\sigma \quad (1)$$

$$PL(d_0) = 10log_{10}(\frac{4\pi d_0}{\lambda})^2 \quad (2)$$

where $PL(d_0)$ is the free space path loss at reference distance d_0, d_0 is equal to 1 m, n is the PLE, d is the distance between TX and RX, χ_σ is the shadow factor which satisfies lognormal distribution with a mean of 0 and standard deviation of σ. For each orientation of RX in the measurement, the directional path loss can be obtained by:

$$PL(d,\varphi)[dB] = P_t[dBm] + G_t[dBi] + G_r[dBi] - P_r(d,\varphi)[dBm] \quad (3)$$

where P_t is the transmitting power, P_r is the directional receiving power, G_t and G_r are the gains of transmitting and receiving antennas, respectively. The PLEs and shadow factors of the directional path loss model for co-polarization and cross-polarization can be obtained from (1) by minimum mean square error (MMSE) fitting.

To eliminate the influence of antenna pattern, omnidirectional path loss model is introduced [19]. The omnidirectional received power is the summation of the directional received power at each azimuth pointing angle of RX:

$$P_{r_{omni}}[mW] = \sum_i P_r(d,\varphi_i)[mW] \quad (4)$$

Substitute the omnidirectional received power into (3), the omnidirectional path loss can be obtained. The CI path loss model shown in (1) is also used to fit the omnidirectional path losses for co-polarization, from which the PLE $n_{(V-V)}$ for co-polarization can be obtained. However, for cross-polarization the close-in reference distance with XPD (CIX) model is applied to fit the omnidirectional path

losses, since it yields a simple model with lower standard deviation [20]. The CIX model can be written as:

$$PL(d)[dB] = PL(d_0)[dB] + 10n_{(V-V)}log_{10}(\frac{d}{d_0}) + XPD[dB] + \chi_\sigma \quad (5)$$

In this equation, instead of solving PLE for cross-polarization, the PLE $n_{(V-V)}$ found from co-polarization is used as a constant, and the XPD is optimized by MMSE fitting to account the additional loss caused by polarization mismatch.

A. PATH LOSS IN CORRIDOR

Fig. 4 and 5 show the measured and fitted directional path losses of corridor in co-polarization and cross-polarization at 26 GHz and 38 GHz, respectively, and the free space path losses are also shown in the figures for reference. Table 2 summarizes the directional PLEs and shadow factors of LOS and NLOS, V-V and V-H polarization at 26 GHz and 38 GHz. At 26 GHz, in V-V polarization the PLEs and shadow factors of LOS and NLOS are 1.61 and 1.51 dB, and 3.80 and 8.38 dB, respectively. The PLE for LOS is smaller than that of free space ($n = 2$) which is caused by the waveguide effect

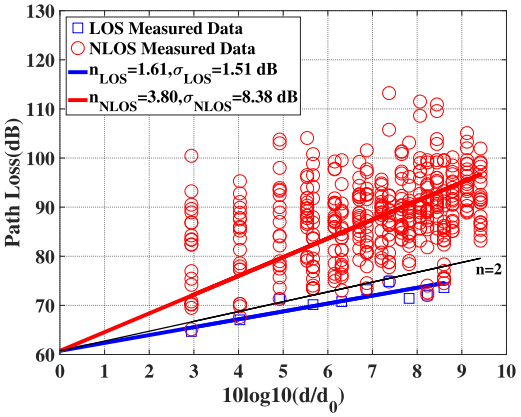

(a)

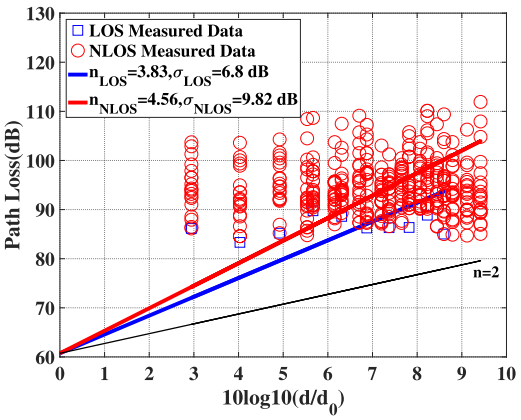

(b)

FIGURE 4. Measured and fitted directional path losses at 26 GHz in corridor. (a) V-V polarization; (b) V-H polarization.

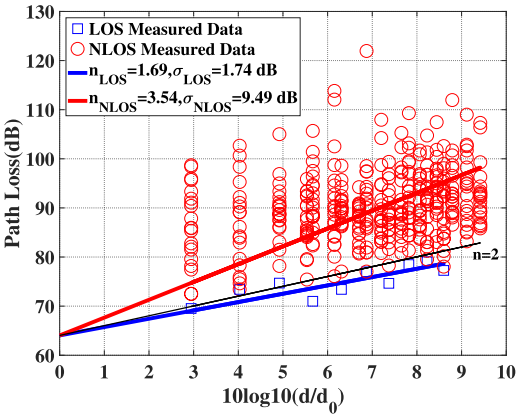

(a)

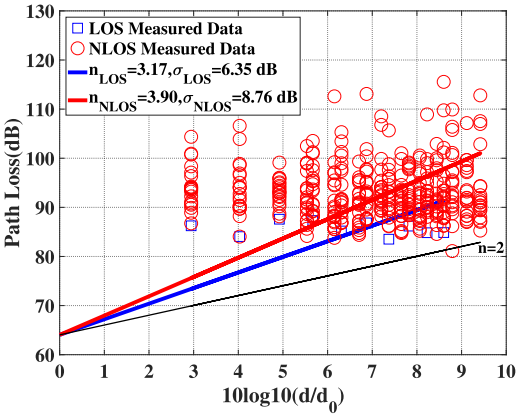

(b)

FIGURE 5. Measured and fitted directional path losses at 38 GHz in corridor. (a) V-V polarization; (b) V-H polarization.

TABLE 2. Directional PLEs and shadow factors of LOS and NLOS, V-V and V-H polarization at 26 GHz and 38 GHz in corridor.

Frequency	Polarization	Scenario	n	σ (dB)
26 GHz	V-V	LOS	1.61	1.51
		NLOS	3.80	8.38
	V-H	LOS	3.83	6.80
		NLOS	4.56	9.82
38 GHz	V-V	LOS	1.69	1.74
		NLOS	3.54	9.49
	V-H	LOS	3.17	6.35
		NLOS	3.90	8.76

in indoor corridor. The PLE and shadow factor of NLOS are much greater than those of LOS, which indicates faster growth and larger fluctuation of path loss in NLOS case due to rich reflected components from the wall and glass window, but lack of LOS component. In V-H polarization the PLEs and shadow factors of LOS and NLOS are 3.83 and 6.80 dB, and 4.56 and 9.82 dB, respectively. Due to the polarization mismatch of the TX and RX antennas, both the PLEs and shadow factor in V-H polarization are greater than those in

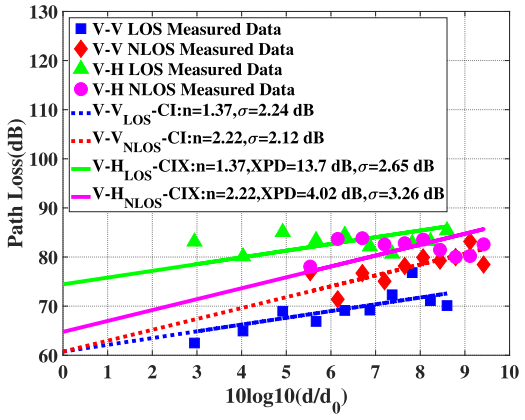

(a)

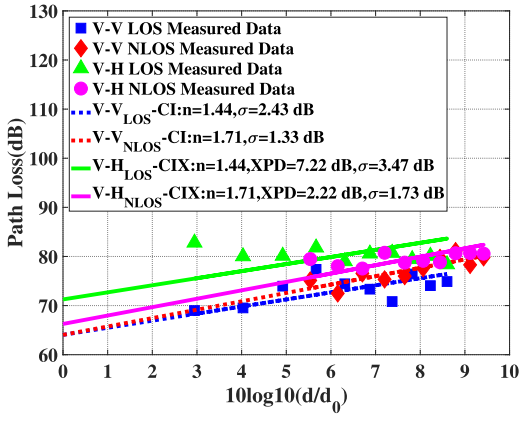

(b)

FIGURE 6. Measured and fitted omnidirectional path losses in corridor at (a) 26 GHz; (b) 38 GHz.

V-V polarization. At 38 GHz, in co-polarization the fitted results are very similar with those at 26 GHz, however in cross-polarization the PLEs and shadow factors are smaller compared to those at 26 GHz which reveals obvious depolarization phenomenon at 38 GHz.

The measured and fitted omnidirectional path losses in corridor at 26 GHz and 38 GHz are shown in Fig. 6(a) and (b), respectively. The CI model in (1) is used to model V-V polarization, and the CIX model in (5) is used to model V-H polarization. Table 3 summarizes the omnidirectional PLEs, XPDs, and shadow factors for each case. At 26 GHz, the omnidirectional PLEs are 1.37 and 2.22 for LOS and NLOS, respectively, and these values are 1.44 and 1.71 at 38 GHz. It can be observed that the omnidirectional PLEs are smaller than their directional counterparts. The XPDs in corridor will be discussed in Section IV.

B. PATH LOSS IN STAIRWELL

To apply the CI path loss model in stairwell, the definition of distance d in (1) needs to be clarified, because of the dog-leg structure of the stairs. It has been pointed out in [35] that when model the path loss of stairwell, the accumulative distance or walking distance should be used instead of the

TABLE 3. Omnidirectional PLEs, XPDs, and shadow factors of LOS and NLOS, V-V and V-H polarization at 26 GHz and 38 GHz in corridor.

Frequency	Polarization	Scenario	n	XPD (dB)	σ (dB)
26 GHz	V-V	LOS	1.37	-	2.24
		NLOS	2.22	-	2.12
	V-H	LOS	1.37	13.7	2.65
		NLOS	2.22	4.02	3.26
38 GHz	V-V	LOS	1.44	-	2.43
		NLOS	1.71	-	1.33
	V-H	LOS	1.44	7.22	3.47
		NLOS	1.71	2.22	1.73

conventional separation distance. In this paper, we define the walking distance as the total tread depth of all the steps between TX and RX, which is proportional to the number of steps.

Fig. 7 and 8 show the measured and fitted directional path losses of stairwell varying with the logarithmic walking distance in V-V and V-H polarization at 26 GHz and 38 GHz, respectively, as well as the free space path losses

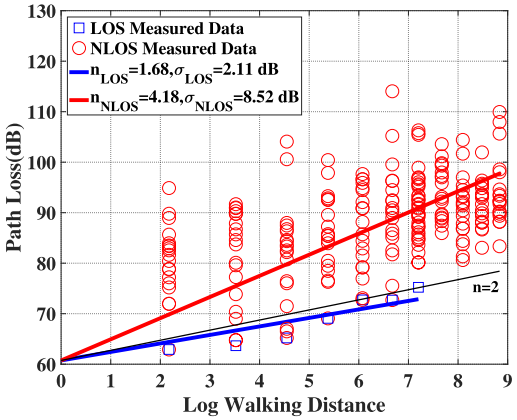

(a)

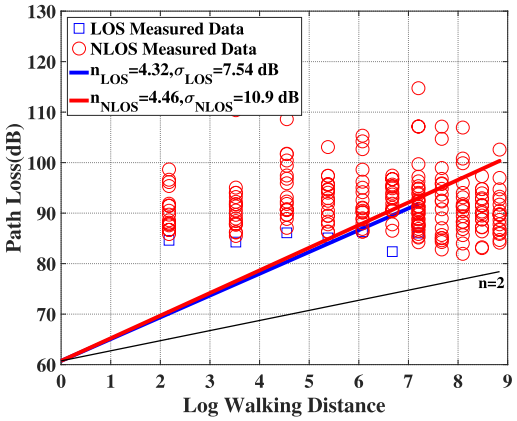

(b)

FIGURE 7. Measured and fitted directional path losses at 26 GHz in stairwellr. (a) V-V polarization; (b) V-H polarization.

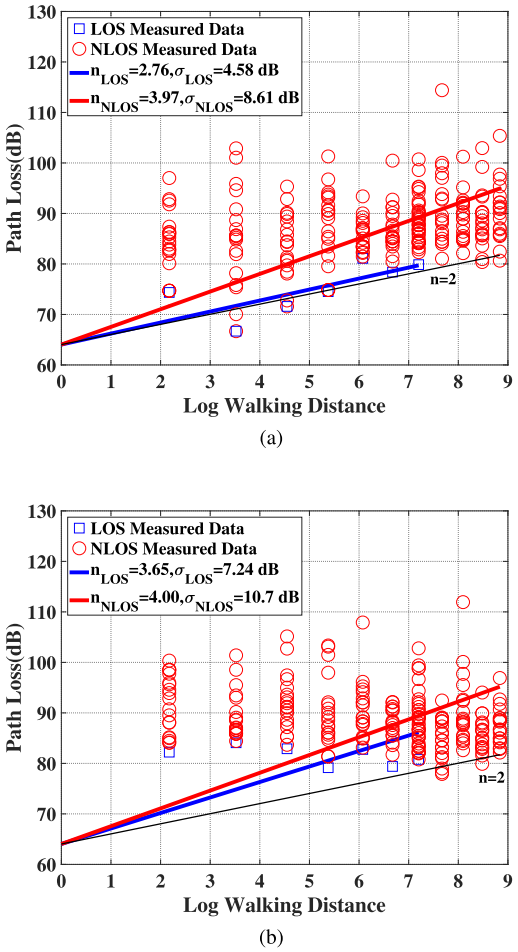

FIGURE 8. Measured and fitted directional path losses at 38 GHz in stairwell. (a) V-V polarization; (b) V-H polarization.

TABLE 4. Directional PLEs and shadow factors of LOS and NLOS, V-V and V-H polarization at 26 GHz and 38 GHz in stairwell.

Frequency	Polarization	Scenario	n	σ (dB)
26 GHz	V-V	LOS	1.68	2.11
		NLOS	4.18	8.52
	V-H	LOS	4.32	7.54
		NLOS	4.46	10.9
38 GHz	V-V	LOS	2.76	4.58
		NLOS	3.97	8.61
	V-H	LOS	3.65	7.24
		NLOS	4.00	10.7

for reference. Table 4 summarizes the directional PLEs and shadow factors of stairwell in different cases. Compared to the corridor, the PLEs of stairwell are larger in most cases. This is attributed to the rich reflection and diffraction introduced by the stairs and railings. Specifically, in S1 section the received signal mainly comes from the LOS component, and the reflected components from walls and stairs also contribute to the total received power. In S2 section, the received signal consists of transmitted component through the railings and stairs, reflected components from the side wall and front wall, diffraction components from edges of stair steps, and even diffuse scattering component. Moreover, it is noted that at 38 GHz, the PLE of NLOS in cross-polarization ($n = 4.00$) is almost the same as that in co-polarization ($n = 3.97$), which is caused by the significant depolarization effect in NLOS scenario.

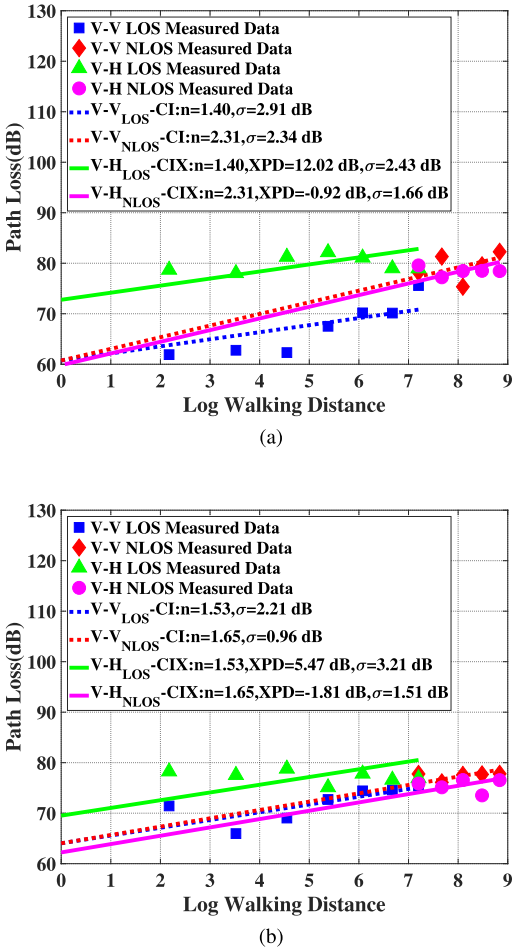

FIGURE 9. Measured and fitted omnidirectional path losses in stairwell at (a) 26 GHz; (b) 38 GHz.

The measured and fitted omnidirectional path losses in stairwell at 26 GHz and 38 GHz are shown in Fig. 9(a) and (b), respectively, in which the walking distance defined above is used. Table 5 lists the omnidirectional PLEs, XPDs, and shadow factors for each case. At 26 GHz, the omnidirectional PLEs are 1.40 and 2.31 for LOS and NLOS, respectively, and these values are 1.53 and 1.65 at 38 GHz. Similar to the directional PLEs, the omnidirectional PLEs of stairwell are larger than those of corridor in most cases. The XPDs in stairwell will be discussed in the next section.

IV. CROSS-POLARIZATION DISCRIMINATION RATIO RESULTS

The polarization state of radio wave can be changed during reflection, diffraction, and scattering, therefore the RX antenna can receive signals even if the polarization of RX

TABLE 5. Omnidirectional PLEs, XPDs, and shadow factors of LOS and NLOS, V-V and V-H polarization at 26 GHz and 38 GHz in stairwell.

Frequency	Polarization	Scenario	n	XPD (dB)	σ (dB)
26 GHz	V-V	LOS	1.40	-	2.91
		NLOS	2.31	-	2.34
	V-H	LOS	1.40	12.02	2.43
		NLOS	2.31	-0.92	1.66
38 GHz	V-V	LOS	1.53	-	2.21
		NLOS	1.65	-	0.96
	V-H	LOS	1.53	5.47	3.21
		NLOS	1.65	-1.81	1.51

antenna mismatches with that of TX antenna. XPD is a critical parameter to quantify the channel depolarization, which is defined as:

$$XPD = P_{r_{co}} - P_{r_{cx}} \tag{6}$$

where $P_{r_{co}}$ is the received power in co-polarization and $P_{r_{cx}}$ is the received power in cross-polarization.

In directional path loss model shown in Table 2 and 4, the difference of the PLEs between V-H polarization and V-V polarization can be used to characterize the average XPD per decade. For example, in corridor environment, the XPDs are 22.2 dB and 7.6 dB per decade for LOS and NLOS at 26 GHz, while they are 14.8 dB and 3.6 dB per decade for LOS and NLOS at 38 GHz. Similarly, the stairwell has a XPD of 26.4 dB and 2.8 dB per decade for LOS and NLOS at 26 GHz, while 8.9 dB and 0.3 dB per decade for LOS and NLOS at 38 GHz. We observed that XPD for LOS is larger than that for NLOS, which indicates the polarization state is preserved in LOS component, and depolarization occurs in NLOS components such as reflection, diffraction, and scattering.

In omnidirectional path loss model shown in Table 3 and 5, the XPD is fitted by CIX model. In corridor, the XPDs are 13.7 dB and 4.02 dB for LOS and NLOS at 26 GHz, and 7.22 dB and 2.22 dB for LOS and NLOS at 38 GHz. In stairwell, the XPDs are 12.02 dB and -0.92 dB for LOS and NLOS at 26 GHz, while they are 5.47 dB and -1.81 dB for LOS and NLOS at 38 GHz. In both corridor and stairwell, the XPD at 38 GHz is smaller than that at 26 GHz, which implies the depolarization effect is stronger at 38 GHz in our specific measured environment. At the same frequency, the XPD in stairwell is smaller than that in corridor, especially the XPD for NLOS scenario in stairwell is close to zero or even negative. Compared to the corridor, there exists more reflection and diffraction surface such as stair steps and iron railings in stairwell environment, which leads to numerous multipath propagations in stairwell and produces manifest depolarization effect. Fig. 10 shows the cumulative distribution functions (CDF) of XPDs obtained from omnidirectional received power in corridor and stairwell at 26 GHz and 38 GHz, and results of LOS and NLOS scenarios are combined in Fig. 10.

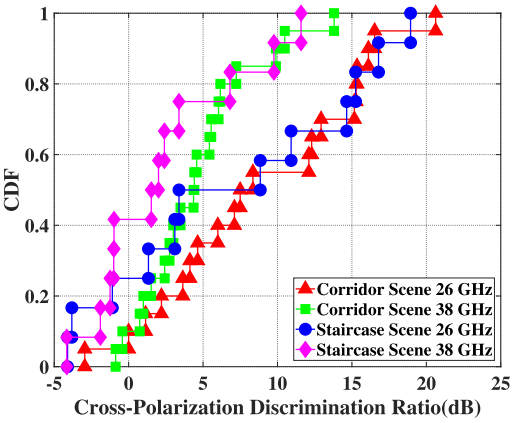

FIGURE 10. CDF of XPDs obtained from omnidirectional received power at 26 GHz and 38 GHz in corridor and stairwell.

V. RMS DELAY SPREAD RESULTS

In multipath channel, signals from different path will arrive at RX with different time delay which causes time dispersion of the channel. RMS delay spread is used to measure the time delay extent of the channel which limits the data rate of communication. RMS delay spread is defined as the standard deviation of the weighted time delay:

$$\sigma_\tau = \sqrt{\overline{\tau^2} - (\overline{\tau})^2} \tag{7}$$

where

$$\overline{\tau^2} = \frac{\sum_k P(\tau_k)\tau_k^2}{\sum_k P(\tau_k)} \tag{8}$$

$$\overline{\tau} = \frac{\sum_k P(\tau_k)\tau_k}{\sum_k P(\tau_k)} \tag{9}$$

where σ_τ is the RMS delay spread, τ_k is the time delay of the kth path, and $P(\tau_k)$ is the received power of the kth path.

The multipath components (MPC) are extracted from power delay profile (PDP). Some measured PDPs in corridor and stairwell at 26 GHz are illustrated in Fig. 11 and Fig. 12, respectively. Strong LOS path components are observed in Fig. 11(a) and Fig. 12(a), which are consistent with the LOS scenario where the TX and RX are aligned on boresight; in contrast, the received powers are much smaller and the delays are larger in Fig. 11(b) and Fig. 12(b), and no LOS components are observed, which are consistent with NLOS scenario where the TX and RX are misaligned. A multipath component is defined as a distinguishable local maximum in the PDP. To detect the local maxima, all peaks of the PDP curve are extracted first with the following condition [46]:

$$P(\tau_k) > P(\tau_k + \Delta), P(\tau_k) > P(\tau_k - \Delta) \tag{10}$$

where Δ is the delay resolution which is 0.25 ns in this paper. Then the local maxima are detected by comparing with the noise threshold and detection threshold. The noise threshold is set to be -90 dBm in this paper, and the detection threshold is defined as a local sliding window average function [47]:

$$T(\tau) = \frac{\varepsilon}{\Lambda} \int_{\tau-\Lambda/2}^{\tau+\Lambda/2} P(x)dx \tag{11}$$

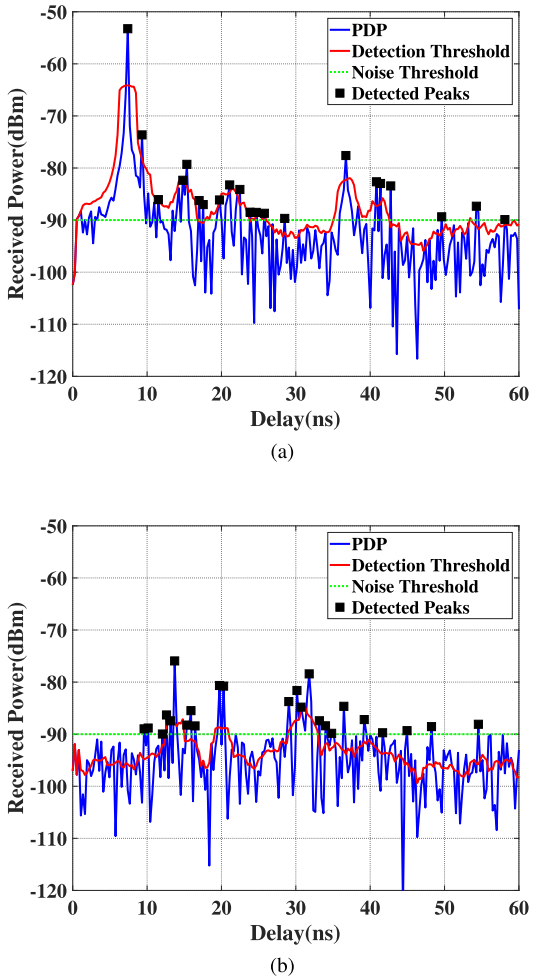

FIGURE 11. Pow delay profiles in V-V polarization at 26 GHz in corridor. (a) LOS; (b) NLOS.

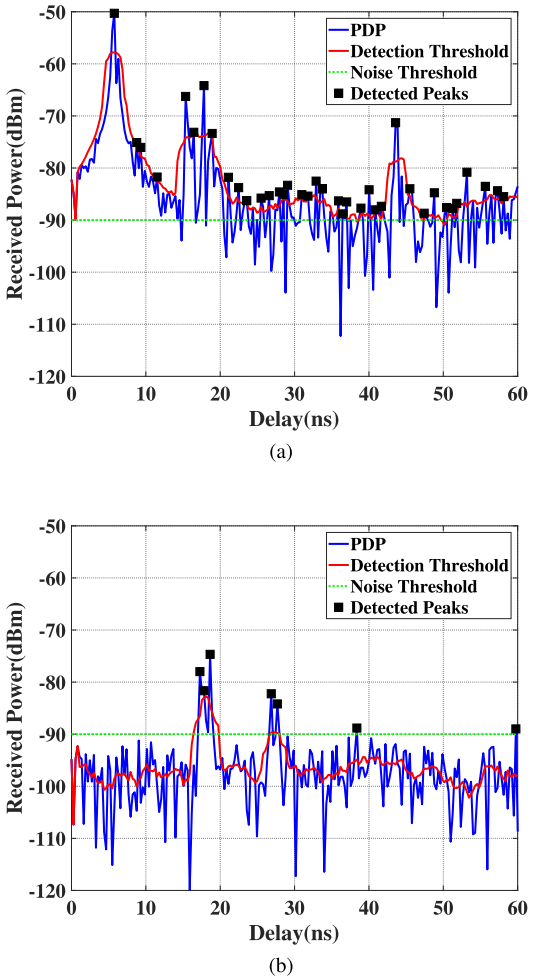

FIGURE 12. Pow delay profiles in V-V polarization at 26 GHz in stairwell. (a) LOS; (b) NLOS.

where Λ is the length of the sliding window over the delay and ε is an offset of the threshold. To avoid the influences of noise and artifacts, a peak is considered to be a multi-path component only if its level is greater than the noise threshold and detection threshold. As an example, the detection threshold, noise threshold and detected MPCs are also shown in Fig. 11 an Fig. 12. Substituting the detected MPCs into (7)-(9), RMS delay spread can be obtained.

A. RMS DELAY SPREAD IN CORRIDOR

RMS delay spreads are measured for all the azimuth pointing angles for each TX-RX location combination. The corridor RMS delay spreads of V-V and V-H polarizations at 26 GHz and 38 GHz are shown in Fig. 13, and it can be observed the RMS delay spread shows no clear dependence on distance. The corresponding CDFs are shown in Fig. 14, which shows that at both 26 GHz and 38 GHz 90% of the RMS delay spreads are less than 18 ns for both LOS and NLOS in any polarization combination.

The average, standard deviation, and maximum of the measured RMS delay spreads in corridor in various cases

TABLE 6. The mean, standard deviation, and maximum values of RMS delay spreads in various cases in corridor.

Frequency	Polarization	Scenario	Mean (ns)	Std. (ns)	Max. (ns)
26 GHz	V-V	LOS	9.10	3.81	20.02
		NLOS	11.86	4.45	25.43
	V-H	LOS	13.06	2.72	19.15
		NLOS	13.01	4.03	21.27
38 GHz	V-V	LOS	10.76	3.95	23.49
		NLOS	14.39	2.29	21.48
	V-H	LOS	14.20	2.69	21.24
		NLOS	14.36	2.35	19.10

are summarized in Table 6. At 26 GHz in V-V polarization, the mean RMS delay spreads are 9.10 ns and 11.86 ns for LOS and NLOS, respectively, while in V-H polarization the mean values are 13.06 ns and 13.01 ns for LOS and NLOS, respectively. In LOS case, the shortest direct path has the strongest power, which reduces the RMS delay spread. In NLOS scenario where the direct path is blocked, the received

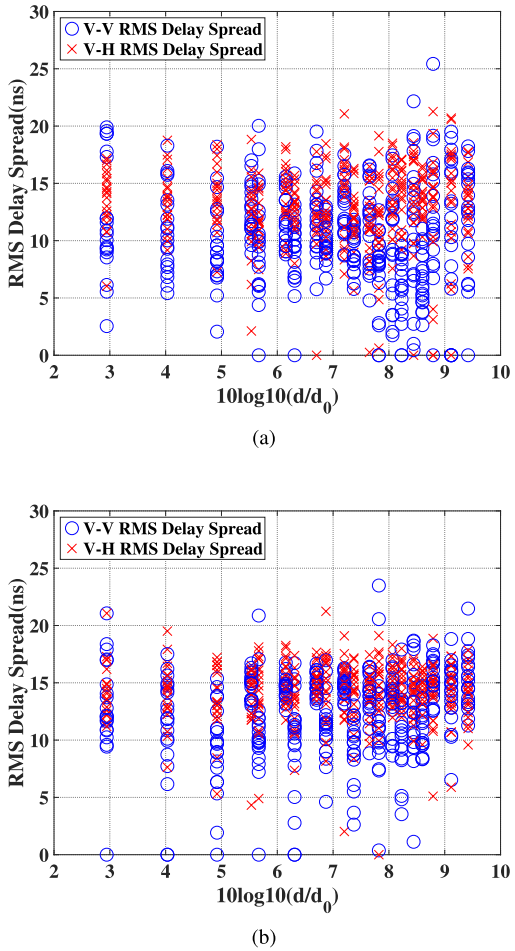

FIGURE 13. Measured RMS delay spreads for V-V and V-H polarizations in corridor. (a) 26 GHz; (b) 38 GHz.

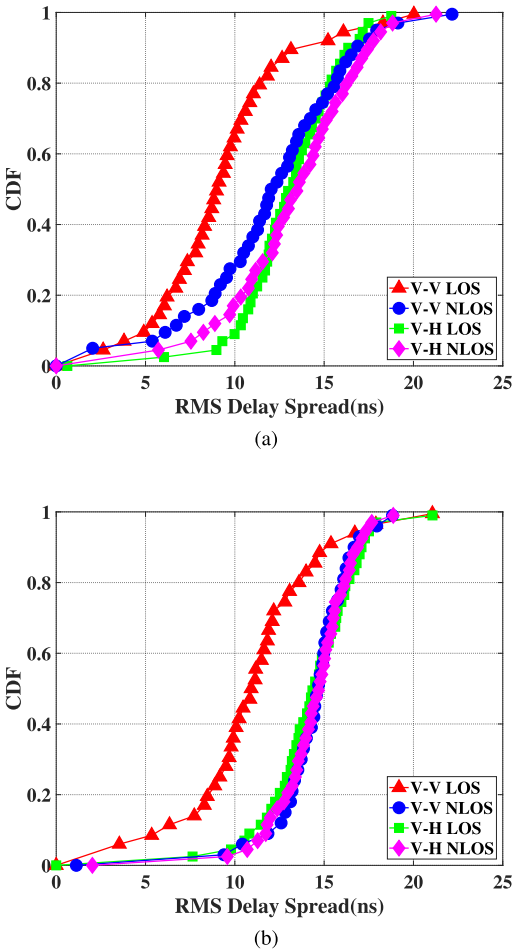

FIGURE 14. CDF of RMS delay spreads for LOS and NLOS in V-V and V-H polarizations in corridor. (a) 26 GHz; (b) 38 GHz.

signals mainly come from reflection, diffraction, and scattering which have larger delay differences and enhance the RMS delay spread. It is also noted that the mean RMS delay spread is larger in V-H polarization compared to that in V-V polarization which is due to the fact that the LOS component in V-H polarization is weakened by the mismatched TX and RX antennas, and more NLOS components in which the polarization reversal occurs can be received. At 38 GHz in V-V polarization, the mean RMS delay spreads are 10.76 ns and 14.39 ns for LOS and NLOS, respectively, while in V-H polarization the mean values are 14.20 ns and 14.36 ns for LOS and NLOS, respectively. Compared to those at 26 GHz, larger RMS delay spreads at 38 GHz indicate more multipaths exist at 38 GHz in the measured corridor.

B. RMS DELAY SPREAD IN STAIRWELL

Fig. 15 shows the RMS delay spreads for V-V and V-H polarizations at 26 GHz and 38 GHz in stairwell, and the corresponding CDFs are shown in Fig. 16. At both 26 GHz and 38 GHz, 90% of the RMS delay spreads are less than 21 ns for both LOS and NLOS in any polarization combination, which are a little larger than those in corridor.

TABLE 7. The mean, standard deviation, and maximum values of RMS delay spreads in various cases in stairwell.

Frequency	Polarization	Scenario	Mean (ns)	Std. (ns)	Max. (ns)
26 GHz	V-V	LOS	11.72	3.73	20.41
		NLOS	13.23	3.97	22.86
	V-H	LOS	14.59	4.17	26.00
		NLOS	16.48	3.67	23.49
38 GHz	V-V	LOS	13.95	3.67	20.81
		NLOS	15.33	3.92	22.87
	V-H	LOS	15.45	5.05	25.32
		NLOS	16.49	2.50	21.00

The average, standard deviation, and maximum of the measured RMS delay spreads in stairwell in various cases are summarized in Table 7. At 26 GHz in V-V polarization, the mean RMS delay spreads are 11.72 ns and 13.23 ns for LOS and NLOS, respectively, while in V-H polarization the mean values are 14.59 ns and 16.48 ns for LOS and NLOS, respectively. At 38 GHz in V-V polarization, the mean RMS delay spreads are 13.95 ns and 15.33 ns for LOS and NLOS,

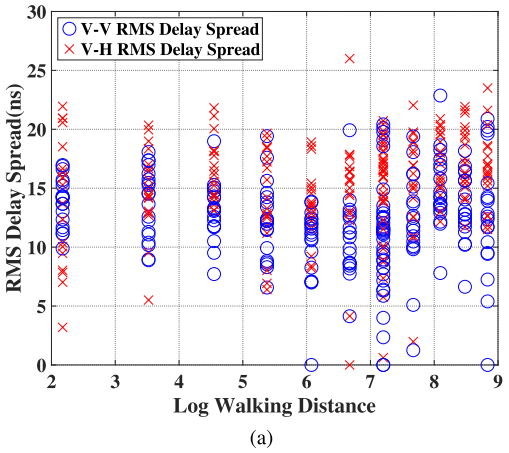

(a)

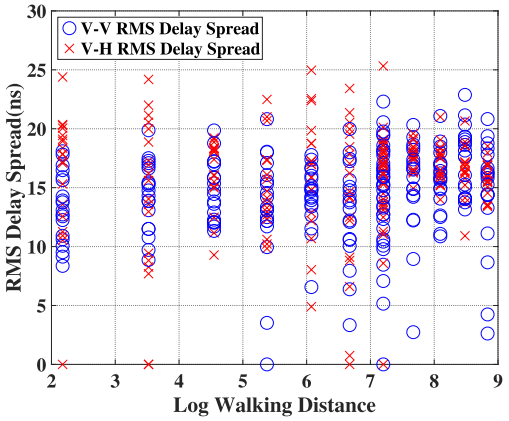

(b)

FIGURE 15. Measured RMS delay spreads for V-V and V-H polarizations in stairwell. (a) 26 GHz; (b) 38 GHz.

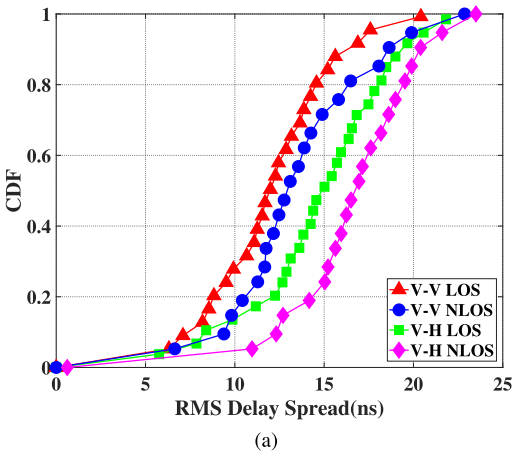

(a)

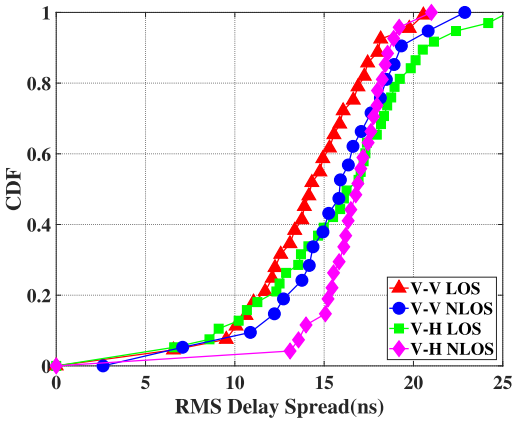

(b)

FIGURE 16. CDF of RMS delay spreads for LOS and NLOS in V-V and V-H polarizations in stairwell. (a) 26 GHz; (b) 38 GHz.

respectively, while in V-H polarization the mean values are 15.45 ns and 16.49 ns for LOS and NLOS, respectively. Similar to the corridor, the RMS delay spread is larger for NLOS than that for LOS in stairwell, also the cross-polarization configuration has larger RMS delay spread than co-polarization in stairwell. Although the overall variation trend of RMS delay spread in stairwell is very similar with that in corridor, we observed that the mean value of RMS delay spread in stairwell is somehow larger than that in corridor for the same configuration, which is due to more NLOS components in stairwell from reflections and scatterings from multiple steps and periodic railing structures.

VI. COMPARISONS WITH OTHER RELATED WORK

The PLEs, shadow factors, XPDs, and mean values of RMS delay spread in corridor and stairwell from different works are listed in Table 8. Although the geometry of environment, the setup of measurement and the method of post-processing are variant among different works, these results are generally consistent and propagation characteristics can be observed from Table 8.

In corridor, the smallest PLE is reported to be 0.6 at 26 GHz [28], while the largest PLE is 5.1 at 28 GHz in V-H polarization for NLOS scenario [20]. In our work, the PLE in corridor ranges from 1.37 to 4.56 at 26 GHz, and 1.44 to 3.90 at 38 GHz in various cases; the shadow factor ranges from 1.51 dB to 9.82 dB at 26 GHz, and 1.33 dB to 9.49 dB at 38 GHz. The XPD is reported to be 10.4 dB to 14 dB at 28 GHz in [20], and 3.4 dB at 38 GHz in [27]. In our work, the XPD is 4.02 dB to 13.7 dB at 26 GHz, and 2.22 dB to 7.22 dB at 38 GHz. The mean value of RMS delay spread in our work ranges from 9.10 ns to 13.06 ns at 26 GHz, and 10.76 ns to 14.39 ns at 38 GHz, which is lager that those reported in [27], [28] but little smaller than those in [20] due to the inherent differences in the geometry and structure of corridor.

In stairwell, the PLE in our work ranges from 1.40 to 4.46 at 26 GHz, and 1.53 to 4.00 at 38 GHz. These values are smaller than those reported in [43], [44], which is may be due to the fact that the measurement distance in our work is relatively small. The XPD and RMS delay spread in stairwell environment are barely reported. In our work, the XPD is from -0.92 dB to 12.02 dB at 26 GHz, and -1.81 dB to 5.47 dB at 38 GHz; the mean value of RMS delay spread ranges from 11.72 ns to 16.48 ns at 26 GHz, and 13.95 ns to 16.49 ns at 38 GHz.

TABLE 8. Comparisons of mmWave indoor propagation characteristics with related works.

Environment	Reference	Frequency (GHz)	Polarization	Scenario	n	σ (dB)	XPD (dB)	Average RMS delay spread (ns)
Corridor	[20]	28	V-V (Directional)	LOS	1.7	2.5	-	17.4
				NLOS	4.4	11.6	-	17.7
			V-H (Directional)	LOS	4.1	8.8	-	17.2
				NLOS	5.1	10.9	-	18.0
			V-V (Omni.)	LOS	1.1	1.8	-	-
				NLOS	2.7	9.6	-	-
			V-H (Omni.)	LOS	1.1	1.5	14.0	-
				NLOS	2.7	9.7	10.4	-
	[27]	28/38	V-V	LOS	0.9/0.8	2.1/2.3	-	4.3/2.3
			V-H	LOS	1.8/1.1	3.8/2.7	11.9/3.4	2.3/1.1
	[28]	28/38	V-V	-	0.6/1.3	3.3/2.4	-	2.3/1.1
	[29]	28	V-V	LOS	1.3	1.3	-	-
				NLOS	3.6	5.7	-	-
	[32]	28	V-V	LOS	1.7	2.4	-	-
				NLOS	2.3	3.4	-	-
	This work	26/38	V-V (Directional)	LOS	1.61/1.69	1.51/1.74	-	9.10/10.76
				NLOS	3.80/3.54	8.38/9.49	-	11.86/14.39
			V-H (Directional)	LOS	3.83/3.17	6.80/6.35	-	13.06/14.20
				NLOS	4.56/3.90	9.82/8.76	-	13.01/14.36
			V-V (Omni.)	LOS	1.37/1.44	2.24/2.43	-	-
				NLOS	2.22/1.71	2.12/1.33	-	-
			V-H (Omni.)	LOS	1.37/1.44	2.65/3.47	13.7/7.22	-
				NLOS	2.22/1.71	3.26/1.73	4.02/2.22	-
Stairwell	[43]	26/38	V-V	-	7.4/7.1	4.4/6.4	-	-
	[44]	26/38	V-V	-	7.52/7.36	9.95/8.98	-	-
			V-H	-	7.79/7.57	6.93/5.55	-	-
	[45]	28	V-V	-	1.9	0.5	-	1.3
	This work	26/38	V-V (Directional)	LOS	1.68/2.76	2.11/4.58	-	11.72/13.95
				NLOS	4.18/3.97	8.52/8.61	-	13.23/15.33
			V-H (Directional)	LOS	4.32/3.65	7.54/7.24	-	14.59/15.45
				NLOS	4.46/4.00	10.9/10.7	-	16.48/16.49
			V-V (Omni.)	LOS	1.40/1.53	2.91/2.21	-	-
				NLOS	2.31/1.65	2.34/0.96	-	-
			V-H (Omni.)	LOS	1.40/1.53	2.43/3.21	12.02/5.47	-
				NLOS	2.31/1.65	1.66/1.51	-0.92/-1.81	-

VII. CONCLUSION

The propagation characteristics of indoor corridor and stairwell at 26 GHz and 38 GHz are investigated by measurement in this paper. Both co-polarization and cross-polarization configurations are considered. The directional and omnidirectional PLEs, shadow factors, XPDs, and RMS delay spreads with associated CDFs are presented for various cases. The results are compared and analyzed with respect to LOS/NLOS scenarios, polarization combinations, frequencies, and environments. For directional path loss, CI model is used in both V-V and V-H polarization, and it is found the directional PLEs in V-H polarization are greater than those in V-V polarization due to the polarization mismatch of the TX and RX antennas in V-H configuration. For omnidirectional path loss, CI model is used in V-V polarization, whereas the CIX model is used in V-H polarization from which the XPD can be obtained. It is found that the omnidirectional PLEs are smaller than directional PLEs, and PLEs for NLOS are greater than those for LOS. Compared to the corridor, PLEs of stairwell are larger in most cases which is attributed to the rich reflection and diffraction introduced by the stairs and railings. We observed that XPD for LOS is larger than that for NLOS,

which indicates the polarization state is preserved in LOS scenario, and depolarization occurs in NLOS scenario. Depolarization phenomenon is manifest in NLOS scenario for higher frequency, and compared to corridor, depolarization is more obvious in stairwell where more scatters exist. In corridor, 90% of the RMS delay spreads are less than 18 ns for all cases, while they are less than 21 ns in stairwell environment. Generally, the RMS delay spread is larger for NLOS than that for LOS, the cross-polarization configuration has larger RMS delay spread than co-polarization, and 38 GHz shows larger RMS delay spreads than 26 GHz in our measured environments. The results in this paper are beneficial to building an efficient and reliable mmWave indoor small cell network.

REFERENCES

[1] A. Ghosh, T. A. Thomas, M. C. Cudak, R. Ratasuk, P. Moorut, F. W. Vook, T. S. Rappaport, G. R. MacCartney, S. Sun, and S. Nie, "Millimeter-wave enhanced local area systems: A high-data-rate approach for future wireless networks," *IEEE J. Sel. Areas Commun.*, vol. 32, no. 6, pp. 1152–1163, Jun. 2014.

[2] T. S. Rappaport, S. Sun, R. Mayzus, H. Zhao, Y. Azar, K. Wang, G. N. Wong, J. K. Schulz, M. Samimi, and F. Gutierrez, "Millimeter wave mobile communications for 5G cellular: It will work!" *IEEE Access*, vol. 1, pp. 335–349, 2013.

[3] M. Shafi, A. F. Molisch, P. J. Smith, T. Haustein, P. Zhu, P. De Silva, F. Tufvesson, A. Benjebbour, and G. Wunder, "5G: A tutorial overview of standards, trials, challenges, deployment, and practice," *IEEE J. Sel. Areas Commun.*, vol. 35, no. 6, pp. 1201–1221, Jun. 2017.

[4] K. Sakaguchi, T. Haustein, S. Barbarossa, E. C. Strinati, A. Clemente, G. Destino, A. Pärssinen, I. Kim, H. Chung, J. Kim, and W. Keusgen, "Where, when, and how mmWave is used in 5G and beyond," *IEICE Trans. Electron.*, vol. E100.C, no. 10, pp. 790–808, Oct. 2017.

[5] T. S. Rappaport, Y. Xing, G. R. MacCartney, A. F. Molisch, E. Mellios, and J. Zhang, "Overview of millimeter wave communications for fifth-generation (5G) wireless networks—With a focus on propagation models," *IEEE Trans. Antennas Propag.*, vol. 65, no. 12, pp. 6213–6230, Dec. 2017.

[6] J. Senic, C. Gentile, P. B. Papazian, K. A. Remley, and J.-K. Choi, "Analysis of E-band path loss and propagation mechanisms in the indoor environment," *IEEE Trans. Antennas Propag.*, vol. 65, no. 12, pp. 6562–6573, Dec. 2017.

[7] A. Bamba, F. Mani, and R. D'Errico, "Millimeter-wave indoor channel characteristics in *V* and *E* bands," *IEEE Trans. Antennas Propag.*, vol. 66, no. 10, pp. 5409–5424, Oct. 2018.

[8] A. Karttunen, K. Haneda, J. Järveläinen, and J. Putkonen, "Polarisation characteristics of propagation paths in indoor 70 GHz channels," in *Proc. 5th Eur. Conf. Antennas Propag. (EuCAP)*, Lisbon, Portugal, 2015, pp. 1–4.

[9] P. F. M. Smulders and A. G. Wagemans, "Frequency-domain measurement of the millimeter wave indoor radio channel," *IEEE Trans. Instrum. Meas.*, vol. 44, no. 6, pp. 1017–1022, Dec. 1995.

[10] T. Manabe, K. Sato, H. Masuzawa, K. Taira, T. Ihara, Y. Kasashima, and K. Yamaki, "Polarization dependence of multipath propagation and high-speed transmission characteristics of indoor millimeter-wave channel at 60 GHz," *IEEE Trans. Veh. Technol.*, vol. 44, no. 2, pp. 268–274, May 1995.

[11] S. Geng and P. Vainikainen, "Millimeter-wave propagation in indoor corridors," *IEEE Antennas Wireless Propag. Lett.*, vol. 8, pp. 1242–1245, 2009.

[12] A. Maltsev, "Characteristics of indoor millimeter-wave channel at 60 GHz in application to perspective WLAN system," in *Proc. 4th Eur. Conf. Antennas Propag.(EuCAP)*, Barcelona, Spain, 2010, pp. 1–5.

[13] C. Gustafson, K. Haneda, S. Wyne, and F. Tufvesson, "On mm-wave multipath clustering and channel modeling," *IEEE Trans. Antennas Propag.*, vol. 62, no. 3, pp. 1445–1455, Mar. 2014.

[14] K. Haneda, J. Järveläinen, A. Karttunen, M. Kyrö, and J. Putkonen, "A statistical spatio-temporal radio channel model for large indoor environments at 60 and 70 GHz," *IEEE Trans. Antennas Propag.*, vol. 63, no. 6, pp. 2694–2704, Jun. 2015.

[15] X. Wu, C.-X. Wang, J. Sun, J. Huang, R. Feng, Y. Yang, and X. Ge, "60-GHz millimeter-wave channel measurements and modeling for indoor office environments," *IEEE Trans. Antennas Propag.*, vol. 65, no. 4, pp. 1912–1924, Apr. 2017.

[16] J. Zhu, H. Wang, and W. Hong, "Large-scale fading characteristics of indoor channel at 45-GHz band," *IEEE Antennas Wireless Propag. Lett.*, vol. 14, pp. 735–738, Dec. 2015.

[17] G. Yue, D. Yu, H. Qiu, K. Guan, L. Yang, and Q. Lv, "Measurements and ray tracing simulations for non-line-of-sight millimeter-wave channels in a confined corridor environment," *IEEE Access*, vol. 7, pp. 85066–85081, 2019.

[18] J. Lee, K.-W. Kim, M.-D. Kim, J.-J. Park, Y. K. Yoon, and Y. J. Chong, "Measurement-based millimeter-wave angular and delay dispersion characteristics of outdoor-to-indoor propagation for 5G millimeter-wave systems," *IEEE Access*, vol. 7, pp. 150492–150504, 2019.

[19] S. Deng, M. K. Samimi, and T. S. Rappaport, "28 GHz and 73 GHz millimeter-wave indoor propagation measurements and path loss models," in *Proc. IEEE Int. Conf. Commun. Workshop (ICCW)*, London, U.K., Jun. 2015, pp. 1244–1250.

[20] G. R. Maccartney, T. S. Rappaport, S. Sun, and S. Deng, "Indoor office wideband millimeter-wave propagation measurements and channel models at 28 and 73 GHz for ultra-dense 5G wireless networks," *IEEE Access*, vol. 3, pp. 2388–2424, 2015.

[21] G. R. MacCartney, S. Deng, and T. S. Rappaport, "Indoor office plan environment and layout-based mmWave path loss models for 28 GHz and 73 GHz," in *Proc. IEEE 83rd Veh. Technol. Conf. (VTC Spring)*, Nanjing, China, May 2016, pp. 1–6.

[22] S. Sun, G. R. MacCartney, and T. S. Rappaport, "Millimeter-wave distance-dependent large-scale propagation measurements and path loss models for outdoor and indoor 5G systems," in *Proc. 10th Eur. Conf. Antennas Propag. (EuCAP)*, Davos, Switzerland, Apr. 2016, pp. 1–5.

[23] T. S. Rappaport, G. R. MacCartney, M. K. Samimi, and S. Sun, "Wideband millimeter-wave propagation measurements and channel models for future wireless communication system design," *IEEE Trans. Commun.*, vol. 63, no. 9, pp. 3029–3056, Sep. 2015.

[24] J. Lee, J. Liang, M.-D. Kim, J.-J. Park, B. Park, and H. K. Chung, "Measurement-based propagation channel characteristics for millimeter-wave 5G Giga communication systems," *ETRI J.*, vol. 38, no. 6, pp. 1031–1041, Dec. 2016.

[25] A. M. Al-Samman, T. A. Rahman, M. H. Azmi, and S. A. Al-Gailani, "Millimeter-wave propagation measurements and models at 28 GHz and 38 GHz in a dining room for 5G wireless networks," *Measurement*, vol. 130, pp. 71–81, Dec. 2018.

[26] L. Zhou, L. Xiao, Z. Yang, J. Li, J. Lian, and S. Zhou, "Path loss model based on cluster at 28 GHz in the indoor and outdoor environments," *Sci. China Inf. Sci.*, vol. 60, no. 8, pp. 25–35, Jun. 2017.

[27] A. M. Al-Samman, T. A. Rahman, M. H. Azmi, M. N. Hindia, I. Khan, and E. Hanafi, "Statistical modelling and characterization of experimental mm-wave indoor channels for future 5G wireless communication networks," *PLoS ONE*, vol. 11, no. 9, Sep. 2016, Art. no. e0163034.

[28] A. M. Al-Samman, T. Abd Rahman, and M. H. Azmi, "Indoor corridor wideband radio propagation measurements and channel models for 5G millimeter wave wireless communications at 19 GHz, 28 GHz, and 38 GHz bands," *Wireless Commun. Mobile Comput.*, vol. 2018, pp. 1–12, Mar. 2018.

[29] A. M. Al-Samman, T. Abd. Rahman, T. Al-Hadhrami, A. Daho, M. N. Hindia, M. H. Azmi, K. Dimyati, and M. Alazab, "Comparative study of indoor propagation model below and above 6 GHz for 5G wireless networks," *Electronics*, vol. 8, no. 1, p. 44, Jan. 2019.

[30] P. Zhang, J. Li, H. Wang, H. Wang, and W. Hong, "Indoor small-scale spatiotemporal propagation characteristics at multiple millimeter-wave bands," *IEEE Antennas Wireless Propag. Lett.*, vol. 17, no. 12, pp. 2250–2254, Dec. 2018.

[31] M. Aborahama, A. Zakaria, M. H. Ismail, M. El-Bardicy, M. El-Tarhuni, and Y. Hatahet, "Large-scale channel characterization at 28 GHz on a university campus in the united arab emirates," *Telecommun. Syst.*, vol. 74, no. 2, pp. 185–199, Jan. 2020.

[32] D. Chizhik, J. Du, R. Feick, M. Rodriguez, G. Castro, and R. A. Valenzuela, "Path loss and directional gain measurements at 28 GHz for non-line-of-sight coverage of indoors with corridors," *IEEE Trans. Antennas Propag.*, vol. 68, no. 6, pp. 4820–4830, Jun. 2020.

[33] B. Ai, K. Guan, R. He, J. Li, G. Li, D. He, Z. Zhong, and K. M. S. Huq, "On indoor millimeter wave massive MIMO channels: Measurement and simulation," *IEEE J. Sel. Areas Commun.*, vol. 35, no. 7, pp. 1678–1690, Jul. 2017.
[34] G. Zhang, K. Saito, W. Fan, X. Cai, P. Hanpinitsak, J.-I. Takada, and G. F. Pedersen, "Experimental characterization of millimeter-wave indoor propagation channels at 28 GHz," *IEEE Access*, vol. 6, pp. 76516–76526, 2018.
[35] C. U. Bas, R. Wang, S. Sangodoyin, T. Choi, S. Hur, K. Whang, J. Park, C. Jianzhong Zhang, and A. F. Molisch, "Outdoor to indoor propagation channel measurements at 28 GHz," *IEEE Trans. Wireless Commun.*, vol. 18, no. 3, pp. 1477–1489, Mar. 2019.
[36] C. H. Teh and H. T. Chuah, "Propagation measurement in a multi-floor stairwell for model validation," in *Proc. 28th URSI Gen. Assem.*, New Delhi, India, 2005, pp. 1–4.
[37] S. Y. Lim, Z. Yun, J. M. Baker, N. Celik, H.-S. Youn, and M. F. Iskander, "Radio propagation in stairwell: Measurement and simulation results," in *Proc. IEEE Antennas Propag. Soc. Int. Symp.*, Charleston, SC, USA, Jun. 2009, pp. 1–4.
[38] S. Y. Lim, Z. Yun, J. M. Baker, N. Celik, H.-S. Youn, and M. F. Iskander, "Propagation modeling and measurement for a multifloor stairwell," *IEEE Antennas Wireless Propag. Lett.*, vol. 8, pp. 583–586, 2009.
[39] S. Y. Lim, Z. Yun, and M. F. Iskander, "Radio propagation measurements in multifloor indoor stairwells," in *Proc. IEEE Int. Conf. Wireless Inf. Technol. Syst.*, Honolulu, HI, USA, Aug. 2010, pp. 1–4.
[40] S. Y. Lim, Z. Yun, and M. F. Iskander, "Propagation measurement and modeling for indoor stairwells at 2.4 and 5.8 GHz," *IEEE Trans. Antennas Propag.*, vol. 62, no. 9, pp. 4754–4761, Sep. 2014.
[41] O. A. Aziz and T. A. Rahman, "Investigation of path loss prediction in different multi-floor stairwells at 900 MHz and 1800 MHz," *Prog. Electromagn. Res. M*, vol. 39, pp. 27–39, Sep. 2014.
[42] V. A. Fono, L. Talbi, O. A. Safia, M. Nedil, and K. Hettak, "Deterministic modeling of indoor stairwells propagation channel," *IEEE Antennas Wireless Propag. Lett.*, vol. 19, no. 2, pp. 327–331, Feb. 2020.
[43] A. M. Al-Samman, T. A. Rahman, M. N. Hindia, and J. Nasir, "Path loss model for indoor emergency stairwell environment at millimeter wave band for 5G network," *Turkish J. Electr. Eng. Comput. Sci.*, vol. 26, no. 6, pp. 3025–3033, Nov. 2018.
[44] A. O. Aldhaibani, T. A. Rahman, and A. Alwarafy, "Radio-propagation measurements and modeling in indoor stairwells at millimeter-wave bands," *Phys. Commun.*, vol. 38, Feb. 2020, Art. no. 100955.
[45] A. Al-Saman, M. Mohamed, and M. Cheffena, "Radio propagation measurements in the indoor stairwell environment at 3.5 and 28 GHz for 5G wireless networks," *Int. J. Antennas Propag.*, vol. 2020, pp. 1–10, Dec. 2020.
[46] A. Karttunen, J. Järveläinen, S. L. H. Nguyen, and K. Haneda, "Modeling the multipath cross-polarization ratio for 5–80-GHz radio links," *IEEE Trans. Wireless Commun.*, vol. 18, no. 10, pp. 4768–4778, Oct. 2019.
[47] K. Haneda, J. Järveläinen, A. Karttunen, M. Kyro, and J. Putkonen, "Indoor short-range radio propagation measurements at 60 and 70 GHz," in *Proc. 8th Eur. Conf. Antennas Propag. (EuCAP)*, The Hague, The Netherlands, Apr. 2014, pp. 634–638.

YUYAN SHEN received the B.S. degree in electronic and information engineering from the Jilin Business and Technology College, in 2018. She is currently pursuing the master's degree with the School of Communication and Information Engineering, Chongqing University of Posts and Telecommunications (CQUPT). Her current research interests include antenna propagation, indoor millimeter-wave propagation measurement, and channel analysis and modeling.

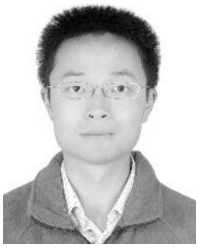

YU SHAO (Member, IEEE) received the B.E. and M.Sc. degrees from Wuhan University, China, in 2009 and 2011, respectively, and the Ph.D. degree from Auburn University, USA, in 2015. In 2016, he was with the Chongqing University of Posts and Telecommunications, where he is currently an Associate Professor with the Communication Department. His current research interests include antennas, radio propagation and channel modeling, computational electromagnetics, and bioelectromagnetics.

XI LIAO (Member, IEEE) received the B.Sc. degree in communication engineering from Hohai University, Nanjing, China, in 2011, and the Ph.D. degree in communication and information engineering from Harbin Engineering University, China, in 2015. Since 2016, she has been a Lecturer with the School of Communication and Information Engineering, Chongqing University of Posts and Telecommunications, China. Her current research interests include twisted radio waves and applications, propagation measurement, and parameter extraction.

HENG ZHANG received the B.S. degree in electronic and information engineering from the Chongqing University of Posts and Telecommunications (CQUPT), in 2018, where he is currently pursuing the master's degree with the School of Communication and Information Engineering. His current research interests include indoor millimeter-wave propagation measurement, channel analysis and modeling, massive MIMO, and beam-forming technology.

JIE ZHANG (Senior Member, IEEE) had studied/worked with Imperial College London, Oxford University, and the University of Bedfordshire, becoming a Lecturer, a Reader, and a Professor, in 2002, 2005, and 2006, respectively. He has been the Chair of Wireless Systems with the Department of Electronic and Electrical Engineering, The University of Sheffield, since 2011. Along with his students/colleagues, he has pioneered research in femto/small cell and HetNets and published some of the earliest and most cited publications in these topics. His Google scholar citations are over 5700. He co-founded RANPLAN Wireless, which is listed on NASDAQ First North and produces a suite of world leading in-building DAS, indoor-outdoor small cell/HetNet network design and optimization tools, including the Ranplan Professional, Tablet and Manager that have been used by the world's largest telecom equipment manufacturers and mobile operators across the globe. His current research interests include data-driven proactive network optimization, millimeter wave small cell communications in the built environments, and modeling and design of smart environments. Since 2005, he has been awarded over 20 grants by EPSRC, and EC FP6/FP7/H2020, including some of world's earliest research projects on femtocell/HetNets.